2018 IEEE-RAS 18th International Conference on Humanoid Robots (Humanoids)
Beijing, China, November 6-9, 2018

Evaluating Robot Manipulability in Constrained Environments by Velocity Polytope Reduction*

Philip Long and Taskin Padir [1]

Abstract— **Robot performance measures are essential tools for quantifying the ability to execute manipulation tasks. Typically, these measures focus on the system's geometric structure and how it impacts the transformation from joint to Cartesian space. In this paper, we propose a new method to evaluate the robot's performance that considers both the system's geometric structure and the presence of obstacles close to or in contact with the robot. This method reduces the manipulator's joint velocity limits by deforming the manipulability polytope to account for obstacles. These constraints are then propagated throughout the chain to get a more representative measure of the end effector's velocity capabilities. The proposed method leads to improved understanding of the robot's capacities in a constrained environment.**

I. INTRODUCTION

As the worldwide energy demand is expected to increase by 50% within the next three decades, nuclear energy will play a critical role in meeting clean energy targets worldwide. However many nuclear facilities are aging and in coming decades hundreds must be decommissioned, a costly and hazardous task. For instance, since 1989, the U.S. Department of Energy has spent over $250 billion of public funds on cleanup. It is now clear that robotics will play a key role in accelerating these cleanup timelines and reducing the costs, by addressing operational needs and challenges in nuclear facilities. Recently, humanoid robots have been proposed to decommission nuclear gloveboxes and hot cells [1], a challenging task due to the environmental constraints. Thanks to its high degree of freedom, a humanoid robot can satisfy the task constraints in multiple configurations. These solutions should not only respect constraints but also maximize robot capability for future operations [2]. Our long term objective is to allow posture optimization, constrained motion planning and supervisory control within nuclear gloveboxes. With this in mind this paper focuses on developing a performance index that evaluates the manipulability of a humanoid's arms operating in such environments.

Robot performance indices have been used for synthesis, manipulator placement and task planning applications. These measures can be classified as local, for instance manipulability [3] or global such as workspace analysis [4]. The former may be used to select a configuration based on a manipulator's inherent capability. The latter can analyze the performance throughout a workspace and thus compare manipulator suitability. A good local index does not imply a good global performance or vice versa [5]. If the workspace is well known, it can be discretized and reachability can be verified for each voxel [4]. However, we focus on a local index that considers both the robot's capabilities and the constraints imposed by the immediate environment.

Robotic research has long focused on extending local measures to include different constraints. For instance, much work has centered on altering the manipulability ellipsoid [3]. In [6] the author proposes to modify the manipulability index using a penalty function based on proximity to positional joint limits. Joint velocity limits are considered in [7] by scaling the Jacobian matrix. The application of contact constraints to the dynamic manipulability of a humanoid's center of mass is developed in [8], [9]. This measure captures the frictional effect, and in [9] a scaling matrix is used to enforce either joint torque or acceleration limits. The work closest to ours is that presented in [4], [10], in which an extended manipulability measure for performance evaluation and grasp selection that considers joint limits and obstacle is proposed. To embed these constraints, the Jacobian is modified by a scaling matrix. Additionally, by workspace discretization, the authors can generate a manipulability map and thus a global index. To achieve this a set of scaled augmented Jacobian matrices is computed that considers workspace movements in all possible Cartesian directions.

A more natural way of representing velocity limits in task directions is provided by manipulability polytopes. First proposed in [11] manipulability polytopes give an exact representation of velocity bounds rather than the approximation provided by ellipsoids [12], [13]. Indeed, polytopes have been shown to be less susceptible to error in redundant cases [14], [15]. Furthermore, task constraints can be easily added to existing polytopes, for instance mobile robot toppling constraints in [16] or friction cones [17]. Thus they may be more suitable to whole body optimization based motion planners [18] than classical manipulability methods. In spite of these advantages, polytopes are less frequently used than their ellipsoid counterparts due to the additional computational cost [10].

In this paper we propose a novel method to measure humanoid performance based on the modification of velocity polytopes. Our objective is to develop an index for robot motion planning and workspace analysis rather than a mea-

*This research is supported by the Department of Energy under Award Number DE-EM0004482, by the National Aeronautics and Space Administration under Grant No. NNX16AC48A issued through the Science and Technology Mission Directorate and by the National Science Foundation under Award No. 1451427.

[1]Philip Long and Taskin Padir are with Department of Electrical and Computer Engineering, Northeastern University, Boston, MA 02115, USA p.long@northeastern.edu, t.padir@northeastern.edu

sure purely based on the kinematic structure. In contrast to previous work, both task space and joint space constraints on each link are taken into account. In constrained environments, task space restrictions imposed by obstacles limit the motion of a link in the serial chain. These constraints also modify the end effector capacity to generate velocity and force even if the end effector itself is located in free space. In our method, the constraints on each link alter the joint velocity polytope, whose effects are in turn transformed to the point of interest. The paper is organized as follows. In Section II, the manipulability is discussed. In Section III, our method is outlined for the general case and an illustrative case study is given. Sections IV describes the experimental validation of this method. Finally, in Section V conclusions are drawn and future work discussed.

II. Manipulability

A. Manipulability Ellipsoid

We consider a n degree-of-freedom manipulator operating in 6 dimensional space. The twist at the end effector frame, $\mathcal{F}_n$, is denoted by $\boldsymbol{\nu}_n$, and is obtained from the kinematic model as

$$\nu_n = \begin{bmatrix} \mathbf{v} \\ \omega \end{bmatrix} = \mathbf{J}_n \dot{\mathbf{q}}, \tag{1}$$

where $\mathbf{J}_n$ is the $6 \times n$ Jacobian matrix defined at $\mathcal{F}_n$. $\mathbf{v}$ and $\boldsymbol{\omega}$ denote the translational and angular velocity respectively. $\dot{\mathbf{q}}$ is the joint velocity vector, $\dot{\mathbf{q}} = [\dot{q}_1, \dot{q}_2 \dots \dot{q}_n]^T$. The manipulability ellipsoid introduced in [3], denoted here as $\mathcal{E}$, measures the robot's capacity to transmit velocities and forces from the joint space to the task space. $\mathcal{E}$ is obtained by considering the joint velocities in the unit sphere i.e.,

$$\dot{\mathbf{q}}^T \dot{\mathbf{q}} \leq 1. \tag{2}$$

By substituting (1) into (2), the task space ellipsoid is described by

$$\mathcal{E} = \{\nu_n^T \left(\mathbf{J}\mathbf{J}^T\right)^{-1} \nu_n \leq 1\}. \tag{3}$$

The principal axes are defined by the eigenvectors of $\mathbf{J}\mathbf{J}^T$ and their magnitude is defined by the singular values of $\mathbf{J}$. Typically the volume of $\mathcal{E}$, given as $w = \sqrt{\mathbf{J}\mathbf{J}^T}$ is used as a performance indicator.

B. Manipulability Polytope

A polytope, $\mathcal{P}$ can be represented as a convex hull of its vertex set ($\mathcal{V}$-representation),

$$\mathcal{P} = \{\mathbf{x} : \mathbf{x} = \sum_{i=1}^{n} \alpha_i \mathbf{y}_i \Big| \alpha_i \geq 0, \sum_{i=1}^{n} \alpha_i = 1\}, \tag{4}$$

where $\mathbf{y}_i$ is the i^{th} element of the vertex set and $\mathbf{x}$ denotes any point contained in $\mathcal{P}$. Alternatively, $\mathcal{P}$ can be defined as the intersection of a finite number of half-spaces ($\mathcal{H}$-representation) as

$$\mathcal{P} = \mathbf{A}\mathbf{x} \leq \mathbf{b}, \tag{5}$$

where $\mathbf{A}$ contains the normals to the half-spaces and $\mathbf{b}$ contains the shifted distance from the origin along the normal. Conversion between representations is possible for instance using the double description method [19].

For a robot of n joints, the joint space polytope, denoted by $\mathcal{Q}$, is a $n-$dimensional polytope that encapsulates all possible joint velocities. In $\mathcal{H}$-representation $\mathcal{Q}$ is given by

$$\begin{bmatrix} \mathbb{I}_n \\ -\mathbb{I}_n \end{bmatrix} \dot{\mathbf{q}} \leq \begin{bmatrix} \dot{\mathbf{q}}_{max} \\ -\dot{\mathbf{q}}_{min} \end{bmatrix}, \tag{6}$$

where $\mathbb{I}_n$ denotes the $n \times n$ identity matrix and $\dot{\mathbf{q}}_{max}$ and $\dot{\mathbf{q}}_{min}$ denote the robot's maximum and minimum joint velocities respectively. The $\mathcal{V}$-representation of $\mathcal{Q}$ contains 2^n vertices in n-dimensional space, whose matrix form is given as

$$\mathbf{Q}_v = \begin{bmatrix} \dot{\mathbf{q}}_1^v \\ \dot{\mathbf{q}}_2^v \\ \vdots \\ \dot{\mathbf{q}}_{2n}^v \end{bmatrix} = \begin{bmatrix} \dot{q}_1^{min} & \dot{q}_2^{min} \dots & \dot{q}_n^{min} \\ \dot{q}_1^{min} & \dot{q}_2^{min} \dots & \dot{q}_n^{max} \\ \vdots & \vdots & \vdots \\ \dot{q}_1^{max} & \dot{q}_2^{max} \dots & \dot{q}_n^{max} \end{bmatrix}. \tag{7}$$

A linear transformation of a polytope always results in another polytope. It follows that a linear transformation applied to $\dot{\mathbf{q}}_j$ is a convex combination of the same linear transformation applied to the vertices. Thus by applying (1) to the vertex set a manipulability polytope, denoted $\mathcal{P}$, is formed for the task space velocities. Partitioning these velocities, to allow for geometrical interpretation with unit homogeneity, [7], the translational velocity vertex set, denoted $\mathbf{V}_v$, contains 2^n vertices in 3-dimensional space, whose matrix form is given as

$$\mathbf{V}_v = \begin{bmatrix} \mathbf{v}_1 & \mathbf{v}_2 & \dots & \mathbf{v}_{2i} \end{bmatrix}^T, \quad \text{where} \quad \mathbf{v}_k = \mathbf{J}_k \, \dot{\mathbf{q}}_k^v. \tag{8}$$

A performance metric, denoted as w_p, is obtained by calculating the enclosed volume. The equivalent ellipsoid's volume is always smaller i.e., $w < w_p$. Indeed, the ellipsoid major axis may not align with the actual direction of the maximal velocity transmission ratio [7].

III. Definition of performance index in constrained environments

In this section, a new method which deforms the manipulability polytope by taking into account obstacles in the robot's workspace is proposed. We posit that a performance index should be guided by two principles

1) The manipulator's maximum velocity in the obstacle's direction should be reduced.
2) The closer the obstacle is to the robot the more pronounced the reduction should be.

To reduce the manipulator's capacities, we propose a potential field method. The *kineostatic dangerfield* [20] can be used to classify the danger associated with a point in the workspace, with respect to the robot's state. In contrast, in our approach, a maximum danger for such a point is enforced by reducing the attainable velocity in that direction. In the following, a variable with the superscript * denotes that the variable is associated with the reduced polytopes.

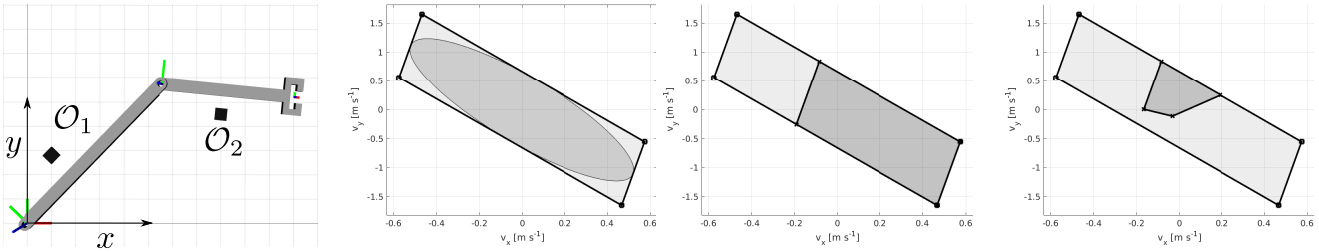

(a) $C1 : \mathbf{q} = [0.8 \ \ -0.9]^T$

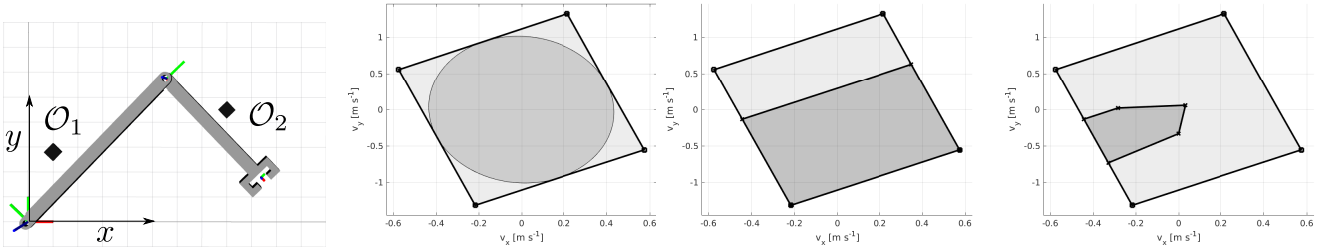

(b) $C2 : \mathbf{q} = [0.8 \ \ -1.6]^T$.

Fig. 1: 2-DOF robot in two configurations, $\mathbf{r}_{o1} = [0.1\,0.28]$ $\mathbf{r}_{o2} = [0.8\,0.45]$. Column 2 shows the manipulability ellipsoid (dark gray) and polytope (light gray). Col. 3 the reduced polytope (dark gray) inscribed in original polytope (light gray) due to one obstacle and Col. 4 the reduced polytope (dark gray) inscribed in original polytope (light gray) due to two obstacles.

A. *Polytope Construction*

The *kineostatic danger field* discretizes the robot's links into l control points (CPs) and the workspace into c cells. The danger field for the j^{th} cell in the environment is calculated as [20]

$$\phi_j = \max_{i=1\ldots l} \left(\frac{1}{\|\mathbf{r}_i - \mathbf{r}_j\|} + \frac{\|\mathbf{v}_i\|(\cos(\angle(\mathbf{r}_i - \mathbf{r}_j, \mathbf{v}_i))}{\|\mathbf{r}_i - \mathbf{r}_j\|^2} \right), \tag{9}$$

where $\mathbf{r}_j$ is the position vector of cell j, $\mathbf{r}_i$ the position vector of CP i on the robot and $\mathbf{v}_i$ is the robot's velocity obtained at i using the kinematic model. $\cos(\angle(\mathbf{r}_i - \mathbf{r}_j, \mathbf{v}_i))$ denotes the cosine of the angle between $\mathbf{v}_i$ and $\mathbf{r}_i - \mathbf{r}_j$. It should be noted that all CPs on the robot's body can contribute to the danger value at cell j rather than simply the closest point to the object. In order to create a system of inequality constraints (9) is re-defined as

$$\forall i, i \in \text{CP}, \quad \phi_j \leq \frac{1}{\|\mathbf{r}_{ij}\|} + \frac{\|\mathbf{v}_i\|(\cos(\angle(\mathbf{r}_{ij}, \mathbf{v}_i))}{\|\mathbf{r}_{ij}\|^2}, \tag{10}$$

where $\mathbf{r}_{ij} = \mathbf{r}_i - \mathbf{r}_j$. Substituting the well-known dot product relation

$$\cos(\angle(\mathbf{r}_{ij}, \mathbf{v}_i)) = \frac{\mathbf{v}_i^T \mathbf{r}_{ij}}{\|\mathbf{v}_i\|\|\mathbf{r}_{ij}\|}, \tag{11}$$

(10) becomes

$$\phi_j \leq \frac{1}{\|\mathbf{r}_{ij}\|} + \frac{\mathbf{v}_i^T \mathbf{r}_{ij}}{\|\mathbf{r}_{ij}\|^3}, \tag{12}$$

Finally, by introducing $\hat{\mathbf{r}}_{ij}$ the normalized unit vector of $\mathbf{r}_{ij}$ after rearrangement (12) becomes

$$\mathbf{v}_i^T \cdot \hat{\mathbf{r}}_{ij} \leq \phi \|\mathbf{r}_{ij}\|^2 - \|\mathbf{r}_{ij}\|, \tag{13}$$

In this paper, rather than creating a danger field for safety purposes, the objective is to study the reduction in performance. Therefore the robot's velocity is reduced until the danger field value at the obstacle location, denoted as o is below a threshold i.e. a defined desired danger value. Equation (13) is re-written as

$$\mathbf{v}_i^T \cdot \hat{\mathbf{r}}_{io} \leq \phi^d \|\mathbf{r}_{io}\|^2 - \|\mathbf{r}_{io}\|, \tag{14}$$

$\mathbf{r}_o$ is the obstacle's position vector with respect to the robot's fixed frame, $\mathcal{F}_w$ and ϕ^d denotes desired danger value. By introducing, (1) the following expression is obtained in configuration space

$$\hat{\mathbf{r}}_{io}^T \, \mathbf{J}_i \dot{\mathbf{q}} \leq \phi^d \|\mathbf{r}_{io}\|^2 - \|\mathbf{r}_{io}\|. \tag{15}$$

$\mathbf{J}_i$ is the $3 \times n$ Jacobian matrix that relates the joint velocities to the translational velocities at point i. If a joint does not contribute to the velocity at CP i the corresponding column of $\mathbf{J}_i$ contains zeros. Hence (15) restricts the maximum velocity for CP i in the direction of the obstacle. Taking into account the l CPs on the robot's body leads to the following set of inequalities

$$\begin{bmatrix} \hat{\mathbf{r}}_{1o}^T \, \mathbf{J}_1 \\ \hat{\mathbf{r}}_{2o}^T \, \mathbf{J}_2 \\ \vdots \\ \hat{\mathbf{r}}_{lo}^T \, \mathbf{J}_l \end{bmatrix} \dot{\mathbf{q}} \leq \begin{bmatrix} \phi^d \|\mathbf{r}_{1o}\|^2 - \|\mathbf{r}_{1o}\| \\ \phi^d \|\mathbf{r}_{2o}\|^2 - \|\mathbf{r}_{2o}\| \\ \vdots \\ \phi^d \|\mathbf{r}_{lo}\|^2 - \|\mathbf{r}_{lo}\| \end{bmatrix}, \tag{16}$$

which for convenience for the k^{th} obtstacle is re-written as

$$\mathbf{J}_{ok} \dot{\mathbf{q}} \leq \mathbf{b}_{ok}. \tag{17}$$

Equation (17) denotes the velocity constraints on all points on the robot due to the k^{th} obstacle. For m obstacles or

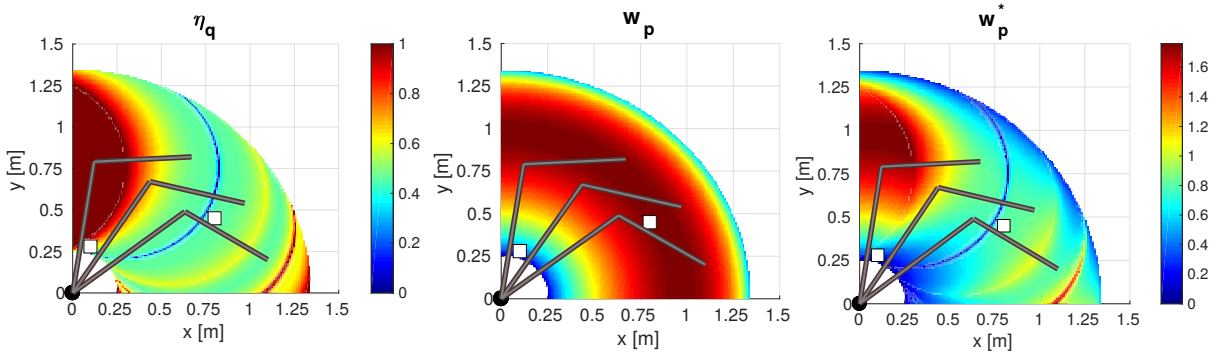

Fig. 2: From left to right: Workspace analysis using joint polytope volume ratio, manipulability polytope volume, reduced manipulability polytope volume. Three configurations are shown $\mathbf{q} = [1.4 \ \ -1.36]^T$, $\mathbf{q} = [0.99 \ \ -1.23]^T$ and $\mathbf{q} = [0.65 \ \ -1.21]^T$.

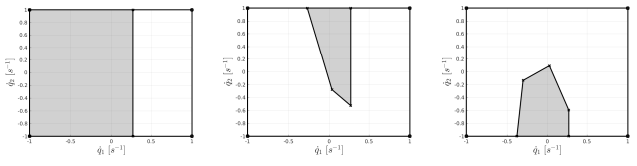

(a) C_{11} and C_{21} (b) C_{12} (c) C_{22}

Fig. 3: Joint Polytopes for planar 2-DOF

danger zones in the robot's workspace and including the constraints defined by (6), this becomes

$$\begin{bmatrix} \mathbf{J}_{o1} \\ \mathbf{J}_{o2} \\ \vdots \\ \mathbf{J}_{om} \\ \mathbb{I}_n \\ -\mathbb{I}_n \end{bmatrix} \dot{\mathbf{q}} \leq \begin{bmatrix} \mathbf{b}_{o1} \\ \mathbf{b}_{o2} \\ \vdots \\ \mathbf{b}_{om} \\ \dot{\mathbf{q}}_{max} \\ -\dot{\mathbf{q}}_{min} \end{bmatrix}. \tag{18}$$

By comparison with (5), it can be seen that (18) is the $\mathcal{H}$-representation of joint space polytope, which is denoted as $\mathcal{Q}^*$. By converting the $\mathcal{H}$-representation to $\mathcal{V}$-representation and transforming the resulting vertices to the task space using (8), a reduced polytope, denoted as $\mathcal{P}^*$ that characterizes the constrained task space performance while also considering joint velocity limits is obtained. It should be noted that this process may result in a dependency between joint velocities. While this gives a true representation of velocity limits, it is often desirable to independently control each joint. If this is the case velocity limits may be obtained by selecting the most restrictive limits in the polytope, i.e. by the largest *hyperrectangle* that can be inscribed in $\mathcal{Q}^*$.

B. Performance Index

By calculating the volume of the reduced polytope $\mathcal{P}^*$ a performance index, denoted w_p^*, for the robot is obtained. However, as this index is configuration dependent, in order to solely analyze the reduction due to environmental constraints the joint polytope must be examined. The n-dimensional joint polytope is composed of a set of n dimensional simplexes. A simplex s is defined by n joint velocity vertices. The volume of the joint polytope is given as sum of volumes of all simplexes, i.e. for a polytope containing k such simplexes

$$w_q = \sum_{s=1}^{k} \left| \frac{1}{n!} \det \begin{pmatrix} \dot{\mathbf{q}}_{s1}^v, & \dot{\mathbf{q}}_{s2}^v, & \dots & \dot{\mathbf{q}}_{sn}^v \end{pmatrix} \right|, \tag{19}$$

where $\dot{\mathbf{q}}_{si}^v$ is the i^{th} vertex of the s^{th} simplex. A performance index is defined as

$$\eta_q = \frac{w_q^*}{w_q}, \tag{20}$$

where w_q^* is the reduced joint polytope's volume. $0 < \eta_q < 1$ is dimensionless and defines the reduction in robot performance due to obstacles and thus is used to complement a chosen metric. Equation (20) is invalid if a joint is immobilized due to constraints since the polytopes exist in different dimensions. Moreover, if the robot has heterogeneous joint types, (20) may no longer be dimensionless. Instead the effect on each joint must be examined, one possible option is given as

$$\eta_r = \frac{1}{n} \sum_{i=1}^{n} \left| \frac{\dot{q}_i^{max*} - \dot{q}_i^{min*}}{\dot{q}_i^{max} - \dot{q}_i^{min}} \right|, \tag{21}$$

which represents the mean performance loss of each joint and should also be used for independent joint control cases.

C. Illustrative 2-DOF planar robot case

The concept is demonstrated for two configurations of a planar manipulator by adding objects and studying the resulting polytopes. The joint velocity limits are given as $\dot{\mathbf{q}}_{min} = [-1.0 \ \ -1.0]$, $\dot{\mathbf{q}}_{max} = [1.0 \ 1.0]$, the link lengths are given as $l_1 = 0.8$, $l_2 = 0.55$. In the following, we refer to C_{ij}, where i and j represent the robot and object configuration respectively. The top row of Fig.1 shows $\mathcal{P}$ and $\mathcal{E}$ at the terminal point, followed by $\mathcal{P}^*$ in the presence of $\mathcal{O}_1$ and (far right) $\mathcal{O}_1$ and $\mathcal{O}_2$. Fig. 3 shows $\mathcal{Q}^*$ inscribed in $\mathcal{Q}$ (a unit square). The addition of $\mathcal{O}_2$ has different effects on both configurations due to its relative location. In Fig.1b, $\mathcal{P}^*$ shows maximum velocity in the negative x and y directions as expected given the object locations. Fig 2, shows a workspace analysis. The workspace is discretized

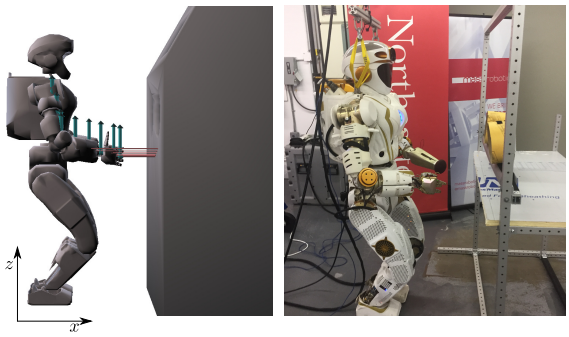

Fig. 4: Experimental setup showing CP (blue) and world frame, $\mathcal{F}_w$. The rays (red) denote obstacles that are close enough to be considered in half-space computations.

into mm^2 cells. At each cell the inverse geometric model is used to obtain the robot's elbow up configuration ($q1 \geq 0$, $q2 \leq 0$). From this configuration the performance indices, η, w_p and w_p^* are calculated. η gives a pure representation of reduced capacities due to obstacles, whereas w_p^* also includes the manipulator's capabilities. Finally, it is interesting to note the blue curve which effectively marks a boundary between the workspace due to the obstacle presence i.e a region the manipulator cannot cross in this configuration.

IV. Experiments

A. Experimental Setup

The experiment consists of inserting the right arm of NASA's *Valkyrie* robot [21] into a glovebox reflecting an example decommissioning action. The setup is shown in Fig.4, on the left the planning environment with a glovebox model and on the real robot with a glovebox mockup. The glovebox model is treated as an obstacle that reduces the robot's velocity capacities. The blue arrows in Fig.4 show the robot's CPs. In order to obtain $\mathbf{r}_{io}$, a ray-casting technique is used. A ray $\mathcal{R}$ is defined as $\mathcal{R} = \mathbf{r}_i + t\begin{bmatrix} \cos(\theta)\sin(\phi) & sin(\theta)\sin(\phi) & cos(\phi) \end{bmatrix}^T$, where $0 \leq \theta \leq 2\pi$ and $0 \leq \phi \leq \pi$. The rays that intersect the glovebox are shown in red in Fig.4 (for clarity only rays along the x-axis are shown). The Jacobian matrix is evaluated at the CP and then projected along the ray to obtain (15). An optimization based motion planner [18] is used to generate a collision free trajectory for the insertion task. During the trajectory execution the model is updated with current configuration values in order to evaluate the manipulators' performance indices.

B. Results

Fig. 5 and Fig. 6 respectively show η defined from (20) and a comparison of w_p and w_p^*. Fig. 8 shows the experiment, divided into four parts, initial configuration, pre-insertion task, insertion and post insertion task. The second row of Fig. 8 shows the manipulability polytope evaluated for the four cases at the right hand. Initially, a slight reduction is seen along the x-axis due to the proximity of the glovebox as shown in Fig. 4. As the hand passes through the port a

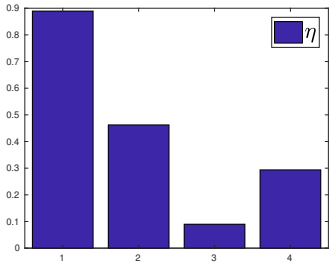

Fig. 5: η_q evaluated for the four configurations. As η_q is defined in the configuration space, it represents the obstacles' effect without considering the arm kinematic transformation.

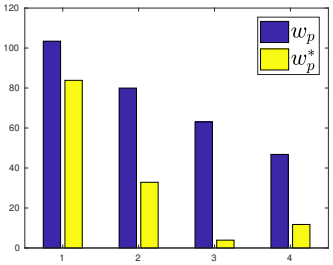

Fig. 6: Comparison of Cartesian Polytope's volume, w_p with w_p^* for the four configurations.

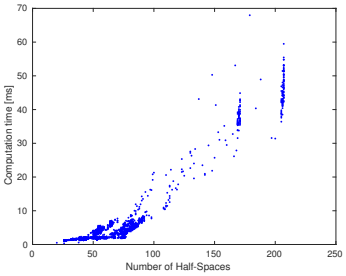

Fig. 7: Computation time versus half-spaces in $\mathcal{Q}^*$.

decrease in velocity capacities is observed. This is also seen in Fig. 5 where $\eta < 0.1$. Fig. 6 shows how w_p diminishes slightly as the arm straightens out whereas the decrease of w_p^* is more pronounced due to the effects of the surrounding obstacle. As the hand emerges on the other side, a gradual increase is noted in the velocity capacity as the translational velocity generated by the wrist joints is no longer constrained by the glovebox port. A corresponding increase in w_p^* and η is seen in part 4 of Fig. 5 and Fig. 6. Finally, Fig. 7 shows the algorithm's computation time for one iteration (including constraint construction, Cartesian transformation and volume computation) $< 70ms$ for ≈ 200 half-spaces (186 detected contacts & joint velocity limits) with an Intel Core i7-7700HQ CPU 2.80GHz $\times$ 8.

V. Conclusion

In this paper, we proposed a new method for quantifying a robot's performance in constrained environments, by limiting

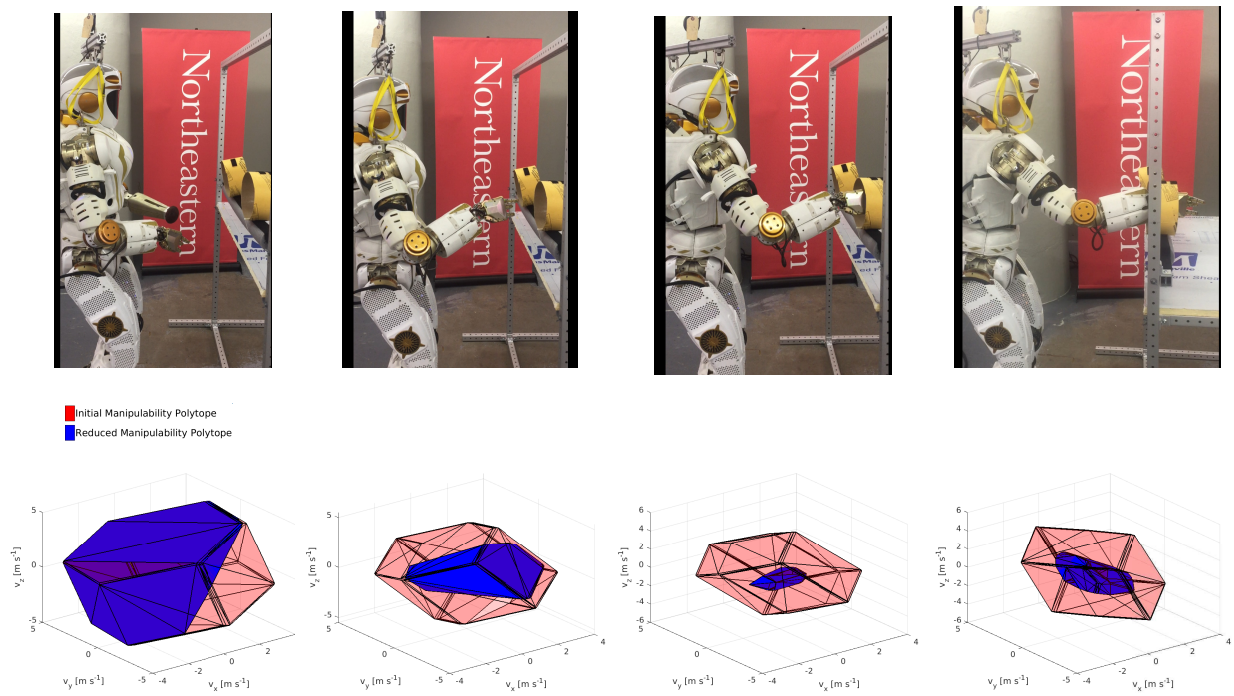

Fig. 8: Top: Valkyrie inserting arm into a glovebox, Bottom: Manipulability Polytope shown in red, reduced polytope shown in blue evaluated at the right hand for the insertion task's four stages.

joint velocities that generate motion towards obstacles. The method is illustrated with a planar case study and it is shown how it can be used to analyze the robot's workspace in cluttered surroundings. Experiments have been performed that demonstrate the method with NASA's Valkyrie robot inserting the right arm into a glovebox. In ongoing work we aim to exploit this index for motion planning purposes for the Valkyrie humanoid robot, for instance as a cost within a contact implicit motion planner framework. Additionally, we aim to consider the humanoid's whole body motion rather than just the right arm.

References

[1] T. Padir, H. Yanco, and R. Platt, "Towards cooperative control of humanoid robots for handling high-consequence materials in glove-boxes," in *WM'17*, WM Symposia, Inc, 2017.

[2] N. Mavrakis, M. Kopicki, R. Stolkin, A. Leonardis, *et al.*, "Task-relevant grasp selection: A joint solution to planning grasps and manipulative motion trajectories," in *IEEE/RSJ Int. Conf. on Intelligent Robots and Systems*, pp. 907–914, IEEE, 2016.

[3] T. Yoshikawa, "Analysis and control of robot manipulators with redundancy," in *Robotics research: the first international symposium*, pp. 735–747, Mit Press Cambridge, MA, 1984.

[4] N. Vahrenkamp and T. Asfour, "Representing the robot's workspace through constrained manipulability analysis," *Autonomous Robots*, vol. 38, pp. 17–30, Jan 2015.

[5] S. Kucuk and Z. Bingul, "Robot workspace optimization based on a novel local and global performance indices," in *IEEE Int. Symposium on Industrial Electronics*, vol. 4, pp. 1593–1598, IEEE, 2005.

[6] M.-J. Tsai, *Workspace geometric characterization and manipulability of industrial robots*. PhD thesis, The Ohio State University, 1986.

[7] J. Lee, "A study on the manipulability measures for robot manipulators," in *IEEE/RSJ Int. Conf. on Intelligent Robots and Systems,*, vol. 3, pp. 1458–1465, IEEE, 1997.

[8] Y. Gu, C. G. Lee, and B. Yao, "Feasible center of mass dynamic manipulability of humanoid robots," in *IEEE Int. Conf. on Robotics and Automation*, pp. 5082–5087, IEEE, 2015.

[9] M. Azad, J. Babič, and M. Mistry, "Dynamic manipulability of the center of mass: A tool to study, analyse and measure physical ability of robots," in *IEEE Int. Conf. on Robotics and Automation*, pp. 3484–3490, IEEE, 2017.

[10] N. Vahrenkamp, T. Asfour, G. Metta, G. Sandini, and R. Dillmann, "Manipulability analysis," in *IEEE-RAS Int. Conf. on Humanoid Robots*, pp. 568–573, IEEE, 2012.

[11] T. Kokkinis and B. Paden, "Kinetostatic performance limits of cooperating robot manipulators using force-velocity polytopes," in *ASME Winter Annual Meeting*, pp. 151–155, 1989.

[12] H. Sekiguchi and K. Ohnishi, "Force capability evaluation methods for bilateral controlled manipulators," in *2017 IEEE Int. Conf. on Mechatronics*, pp. 111–116, IEEE, 2017.

[13] R. Finotello, T. Grasso, G. Rossi, and A. Terribile, "Computation of kinetostatic performances of robot manipulators with polytopes," in *IEEE Int. Conf. on Robotics and Automation, 1998*, vol. 4, pp. 3241–3246, IEEE, 1998.

[14] S. Krut, F. Pierrot, *et al.*, "Velocity performance indices for parallel mechanisms with actuation redundancy," *Robotica*, vol. 22, no. 02, pp. 129–139, 2004.

[15] A. Ajoudani, N. G. Tsagarakis, and A. Bicchi, "On the role of robot configuration in cartesian stiffness control," in *IEEE Int. Conf. on Robotics and Automation, 2015*, pp. 1010–1016, IEEE, 2015.

[16] T. Rasheed, P. Long, D. Marquez-Gamez, and S. Caro, "Tension distribution algorithm for planar mobile cable-driven parallel robots," in *Cable-Driven Parallel Robots*, pp. 268–279, Springer, 2018.

[17] S. Caron, Q.-C. Pham, and Y. Nakamura, "Zmp support areas for multicontact mobility under frictional constraints," *IEEE Transactions on Robotics*, vol. 33, no. 1, pp. 67–80, 2017.

[18] X. Long, M. Wonsick, V. Dimitrov, and T. Padir, "Anytime multi-task motion planning for humanoid robots," in *IEEE/RSJ Int. Conf. on Intelligent Robots and Systems,*, IEEE, 2017.

[19] K. Fukuda and A. Prodon, "Double description method revisited," in *Combinatorics and computer science*, pp. 91–111, Springer, 1996.

[20] B. Lacevic and P. Rocco, "Kinetostatic danger field-a novel safety assessment for human-robot interaction," in *IEEE/RSJ Int. Conf. on Intelligent Robots and Systems*, pp. 2169–2174, IEEE, 2010.

[21] N. A. Radford, P. Strawser, K. Hambuchen, J. S. Mehling, W. K. Verdeyen, A. S. Donnan, J. Holley, J. Sanchez, V. Nguyen, L. Bridgwater, *et al.*, "Valkyrie: Nasa's first bipedal humanoid robot," *Journal of Field Robotics*, vol. 32, no. 3, pp. 397–419, 2015.